Drop deformation in a planar elongational flow: impact of surfactant dynamics

Julian Wailliez, Paul Regazzi, Anniina Salonen, Paul G Chen, Marc Jaeger, Marc Leonetti, Emmanuelle Rio

Drop deformation in a planar elongational flow: impact of surfactant dynamics

Julian Wailliez,[†a] Paul Regazzi,[†b] Anniina Salonen,[a] Paul G. Chen,[c] Marc Jaeger,[c] Marc Leonetti[b] and Emmanuelle Rio[*a]

Drops in extensional flow undergo a deformation, which is primarily fixed by a balance between their surface tension and the viscous stress. This deformation, predicted and measured by Taylor on millimetric drops, is expected to be affected by the presence of surfactants but has never been measured systematically. We provide a controlled experiment allowing us to measure this deformation as a function of the drop size and of the shear stress for different surfactants at varying concentrations. Our observation is that the deformation predicted by Taylor is recovered at zero and high surfactant concentration, whereas it is smaller at concentrations close to the critical micellar concentration. This is in contradiction with the existing analytical models. We develop a new analytical model, taking into account the surfactant dynamics. The model predicts a transition between a deformation similar to the one of a pure liquid and a smaller one. We show that the transition is driven by a parameter K_L, which compares adsorption and desorption dynamics. Finally, the concentration C^*, at which we observe this transition in the extensional flow is in good agreement with the one predicted by independent measurement of K_L.

1 Introduction

Two-phases liquid/fluid dispersions, such as emulsions and foams, are ubiquitous in a wide range of applications ranging from food industry to cosmetics or structural materials.[1] Since these materials are thermodynamically unstable, they tend to evolve towards complete phase separation, which can be slowed down by the addition of surfactants to stabilize the interfaces.

The description of the stability and the evolution of interfaces loaded with surfactants requires a fine description of their dynamics, which includes diffusion in the bulk and at the interface, convection and adsorption/desorption barriers. A precise understanding of the liquid flow is thus needed to describe the convection. Additionally, the presence of surfactants at the interfaces confers an additional surface stress, which impacts the flow.[2–4]

A comprehensive description of a given experimental situation thus requires a fine control of the liquid flow in the limit of a low Reynolds number regime, which can easily be achieved in microfluidics. A key advantage is the ability to directly compare experimental and theoretical results. A known efficient configuration is the deformation of a deformable particle in a planar extensional flow,[5,6], *i.e.*, droplets,[7–10] vesicles,[10,11] polymer or DNA,[12,13] cells[14–16] and microcapsules.[17] Beyond the mastered hydrodynamic stress, one advantage compared to shear flow is the presence of a stagnation point to trap the particle and study it. Nevertheless, similar results can be achieved in microfluidics but with alternative flow such as localized single or successive constrictions.[10,15,16]

Here, we focus on the deformation of a drop of radius R in an extensional flow, historically proposed by Sir Taylor.[7] He demonstrated analytically that in the limit of small deformations with respect to the initial drop radius and a low Reynolds number, the drop shape is an ellipsoid of semi-axes L and S: $|L-S| \ll R$. He introduced the so-called Taylor parameter $D_T = \frac{L-S}{L+S}$. Other assumptions are the negligible effect of buoyancy and the lack of any walls, *i.e.*, the single drop can be considered in an infinite viscous medium. We limit the description to the case where the continuous phase has a viscosity η much larger than the dispersed one. For pure liquids, with an interfacial tension γ, the shape of a drop of initial radius R is fixed by a balance between the shear rate $\dot{\varepsilon}$ and surface tension, leading to

$$D_T = \Xi \mathrm{Ca}, \tag{1}$$

where $\mathrm{Ca} = \frac{\eta \dot{\varepsilon} R}{\gamma}$ is the capillary number and $\Xi = 2$. $\dot{\varepsilon}$ and γ are respectively the elongation rate and the surface tension. The four-roll experiment developed by Taylor gave measurements in agreement with this prediction for millimetric drops.[7] Similar results have been obtained in a microfluidic circuit very recently by Lee *et al.*[8] in the presence of surfactants at high concentration. In this case, the surfactant dynamics are expected to be fast compared to the shear rate so that the surface tension remains constant and homogeneous in time, and the interfaces can be described the ones of pure liquids.

In the 90s, theoretical studies led to predictions for the Taylor deformation in extensional flows, for interfaces loaded with surfactants. Leal and Stone[9] explored the limit, in which the surfactants can be considered as insoluble. In this limit, the prefactor Ξ in the Taylor deformation (eqn (1)) is expected to vary between 2 and 2.5. This means that the deformation is always larger in the presence of insoluble surfactants compared to pure interfaces with the same surface tension. The reason is that the surfactants tend to accumulate at the tip of the drop due to convection, which leads to a local decrease of the surface tension so that the tip becomes easier to deform.

Theoretical developments have proposed that the existence of a surface viscosity can also affect the deformation.[18] In this case, the deformation can be smaller or larger than the one predicted by Taylor for free interfaces.

For soluble surfactants, their dynamics must also be taken into account. In a solution of volume concentration C the repartition of surfactants between surface and volume can be described by

[a] *Université Paris-Saclay, CNRS, Laboratoire de Physique des Solides, 91405 Orsay, France. E-mail: emmanuelle.rio@universite-paris-saclay.fr*
[b] *Aix Marseille Univ, CNRS, CINaM, Marseille, France.*
[c] *Aix Marseille Univ, CNRS, Centrale Med, M2P2, Marseille, France.*
† These authors contributed equally to this work.

an isotherm, such as the one of Langmuir:

$$\Gamma_{eq} = \Gamma_\infty \left(\frac{K_L C}{1 + K_L C} \right), \quad (2)$$

where Γ_{eq} and Γ_∞ are respectively the equilibrium and the maximal surfactant surface concentration and K_L is a parameter, which results from the balance between adsorption and desorption. Together with the Gibbs isotherm, this leads to a state equation. For example, the Szyszkowski equation allows linking the surface tension and the surface concentration:[19]

$$\gamma = \gamma_0 + nRT\Gamma_\infty \ln(1 - \Gamma/\Gamma_\infty) \quad \text{(Szyszkowski)}, \quad (3)$$

with $n = 1$ for neutral and $n = 2$ for ionic surfactants. γ_0 is the interfacial tension for a clean interface, *i.e.*, without surfactants. In the following, in order to be as general as possible, we introduce the Gibbs elasticity:

$$E_s = nRT\Gamma_\infty. \quad (4)$$

The influence of adsorption/desorption dynamics has been taken into account by K. Stebe and her collaborators in simulations, and they have obtained a wide variety of behaviors, with different factors Ξ in the linear regime.[20–22]

Different articles focused on the impact of surfactants on drop deformation, with aim of better controling and optimizing the generation of emulsions. In an extensional flow, Milliken *et al.*[23,24] conclude that it is difficult to predict drop deformation because of the dynamics of surfactants, which leads to tip-streaming. Hu and Lips[25] have quantified the effect of tip-streaming by measuring the difference between the actual drop shape and an ellipse allowing the best shape fit to be obtained. A recent study[8] allowed demonstrating that, at high surfactant concentration (many times the CMC – critical micellar concentration), the deformation can be explained by surface tension. There have been studies in other geometries showing that the impact of surfactants can be explained by the dynamic surface tension[16] or by a subtle interplay between surface viscosity and elasticity.[15] Finally, to our knowledge, these predictions have never been tested in the literature in this geometry.

We thus developed a microfluidic device to create a controlled extensional flow around a sub-millimetric drop. We measured the Taylor deformation as a function of the surfactant concentration for various surfactants. Our main observation is that the prefactor Ξ is smaller than 2 most of the time, which disagrees with the existing analytical models. The team of K. Stebe[20–22] demonstrated that such small prefactors can appear in the presence of bulk surfactant dynamics. Following these results, we propose an analytical model, which takes into account surfactant adsorption/desorption and is in agreement with our experimental data.

2 Experimental Setup

2.1 Materials

To simplify the theoretical description of our experiments, we want to work at small enough Reynolds numbers $\mathrm{Re} = \frac{\rho \dot{\epsilon} R L_c}{\eta}$, with liquid density ρ and canal size L_c, to be in the lubrication approximation and at high enough capillary numbers to observe measurable deformations. The choice of a water in oil dispersion allows capillary numbers up to 10^{-1} to be reached, keeping the Reynolds number smaller than 2×10^{-3}. The drawback is that these emulsions are highly unstable. However, as we want to work with single drops, this is not really a problem, but it does require us to work with dilute emulsions. This avoids collisions, which would lead to coalescence.

2.1.1 Characterization of the oil phase

For the external oil phase, we used two methyl-terminated silicone oils from CarlRoth, one with a viscosity of 1 Pa s and the other with a viscosity of 0.5 Pa s. The viscosity of these oils is sensitive to temperature; thus, it has been measured with a double gap Couette rheometer (Anton Paar 301) as a function of temperature for shear rates in the range 0.5–6 s^{-1}. The oils have a Newtonian behavior in this range, and the viscosity used has been adjusted for each experiment depending on the atmospheric temperature measured during the experiment. Their density of $\rho = 0.98 \pm 0.05$ g cm^{-3}, close to that of water, allows sedimentation of water droplets in the channels to be avoided. The drawback is that it leads to high uncertainty in the density contrast and consequently in surface tension measurement, as we will comment later.

2.1.2 Choice of the aqueous phase

The different surfactants used are listed in Table 1. To explore different surfactants, we selected the family of trimethylammonium bromide (TAB) with two different chain lengths: decyltrimethylammonium bromide (C_{10}TAB) and tetradecyltrimethylammonium bromide (C_{14}TAB). Both were purchased from Sigma Aldrich and further purified through recrystallization.[26] They have the advantage of being widely used in the literature and being chemically stable in time. Additionally, they all have the same hydrophilic head group, so that they mostly differ because of their solubility, as seen in Table 1, where the CMC varies over three orders of magnitude. We also used a Gemini surfactant, which is a non-commercial dimer of dodecyltrimethylammonium bromide (C_{12}TAB) synthesised and given to us by Martin In (Montpellier).[27] The solutions are prepared by dissolving the surfactant in ultrapure water (resistivity = 18.2 MΩ cm).

Table 1 For the different surfactants listed in column 1, column 2 gives the critical micellar concentration (CMC) in mM, and column 3 the molar mass in g mol^{-1}. The values of K_L are obtained by fitting the data of Fig. 1 by eqn (5)

Surfactant	CMC mM	M g mol^{-1}	K_L m^3 mol^{-1}
C_{10}TAB	66	279.16	5.9×10^4
C_{14}TAB	3.6	336.4	1.14×10^6
Gemini	0.97	614.66	5.32×10^6

2.1.3 Measure of the interfacial tension

The interfacial tension is measured for oil/surfactant solution interface using a home-made pendant drop experiment. The drop is deformed by the balance between gravity and capillary forces. To account for the small density ratio, a small needle is used to enhance the ratio between the gravity and the capillary forces and to

obtain a drop with a high enough deformation to be measured accurately. We us a PHLOX (LedW-BL-50 × 50-LLUBQ-IR-24V) lamp for uniform and powerful lighting conditions. The pictures are taken using a Basler camera with a telecentric lens (Edmund optics, CompactTL) to obtain sharp contours. The drop shape is fitted by the pendant drop plugin in Fiji.[28] Another difficulty is that the oil is viscous so that it takes a long time to relax into its equilibrium shape (around 3 minutes). The data are thus obtained at long times, once equilibrium is reached, which prevents the measure of dynamical surface tension. However, this time is comparable but is smaller than the time for a drop to travel along the tube between its generation and the measurement cell (around 5 minutes). This ensures that surface tension has reached equilibrium when we measure drop deformation. Due to the lack of accuracy in the density contrast, this gives a surface tension with error bars of 6 mN m^{-1}. The obtained interfacial tensions are plotted for each surfactant system in Fig. 1. Injecting eqn (2) in eqn (3) allows to express the surface tension as a function of the concentration:

$$\gamma - \gamma_0 = -RT\Gamma_\infty \ln(1 + K_L C). \quad (5)$$

The surface tension curves in Fig. 1 are then fitted by eqn (5) using K_L as a fitting parameter and plotted in Fig. 1 together with experimental data. The fitted values of K_L are listed in Table 1.

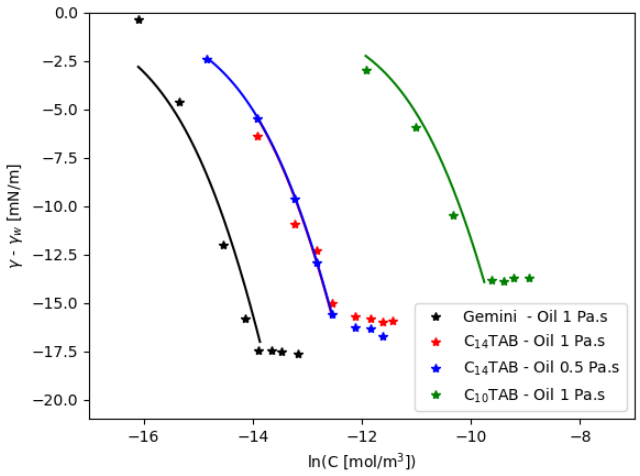

Fig. 1 Surface tension measured using the pendant drop method for each surfactant/oil system. The continuous line is a fit of the data at concentration smaller than the CMC using the Frumkin equation (eqn (5)).

2.2 Experimental setup

Our millifluidic chip is built in transparent plexiglass, chosen because it ages very slowly in ambient light and possesses a high rigidity that varies little with temperature. This avoids channel deformation under fluid stress.

2.2.1 Drop generation

A T-junction (Fig. 2b) is used to generate water-in-oil drops. The principal channel is a square channel with a size $L_c = 2$ mm. It is joined by a perpendicular one, in which a tapered glass capillary is inserted. To avoid droplet coalescence, a diluted emulsion is required. To obtain such an emulsion, we make a chip, in which drops of chosen size can be generated at the push of a button. To achieve this, an Elveflow OB1-type pressure controller is connected to the secondary channel. It is used to apply manually an over-pressure during the chosen time, which results in the generation of a single drop. Direct visualization allows stopping the generation when a drop of the right size is obtained and choosing the onset of the generation of the next one once the precedent is far enough. We then obtain a dilute polydisperse emulsion (Fig. 2a), which flows toward the chamber with the extensional flow configuration.

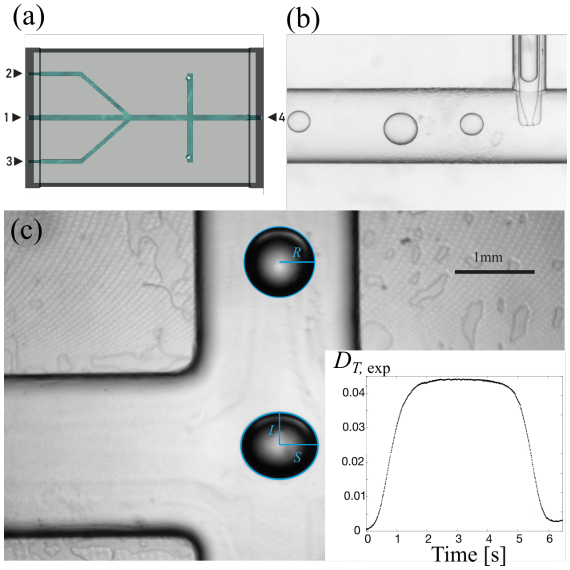

Fig. 2 (a) Millifluidic chip to create the extensional flow. Inlet 1 is used to inject the emulsion. Inlet 2 and 3 are used to dilute the emulsion at will and choose the flowrate and thus the capillary number of the experiment. Inlet 4 allows injection of the counter-flow to balance the flows of channels 1, 2 and 3 and generation of the extensional flow. (b) Visualization of the T-junction, in which three droplets of different sizes have been generated. (c) Image of a circular drop of radius R entering the extensional flow and deforming at the center, becoming an ellipse of principal radii L and S. The three lengths, measured by image treatment, allow calculation of $D_{T,exp}$, which is plotted in the inset as a function of time. It reaches a maximum and remains stable during a few seconds, because the drop is stuck at the stagnation point. The Taylor deformation is measured at the maximum.

2.2.2 Planar elongational flow

The planar elongational flow is a symmetrical (cross-shaped) flow with a point of zero velocity at its center, where the drop will be maintained and where it reaches a stationary deformation regime. To create such a flow, we need to inject a given flow rate through two opposite channels. The flow continues in both other channels, which are at atmospheric pressure. To do so, we machined a PMMA sheet to obtain channels measuring 2 mm by

2 mm, whose structure is shown in Fig. 2(a). Input 1 is used to inject the emulsion. Inputs no 2 and no 3 allow injection of the continuous phase at a chosen flowrate, so that we can modify the capillary number of the flow, with no impact on drop generation. These two entrances also make it easy to center the drops in the flow. Input 4 is used to inject the continuous phase that will constitute the counter-flow. The injection rate of the no 4 must correspond to the sum of the injection rates of inlets no 1, 2 and 3. The two outlets at the extremity of the perpendicular channels are at atmospheric pressure. The different flowrates are controlled by a syringe pump AL1000, World Precision Instruments for inlets 1, 2 and 3 and a syringe pump D-401833, Harvard Apparatus for inlet 4. We consider that the flowrate injected in inlet 4 is correct when we observe that drops arriving in the elongational flow cell are stable for a few seconds. In this case symmetry has been achieved (see inset in Fig. 2c).

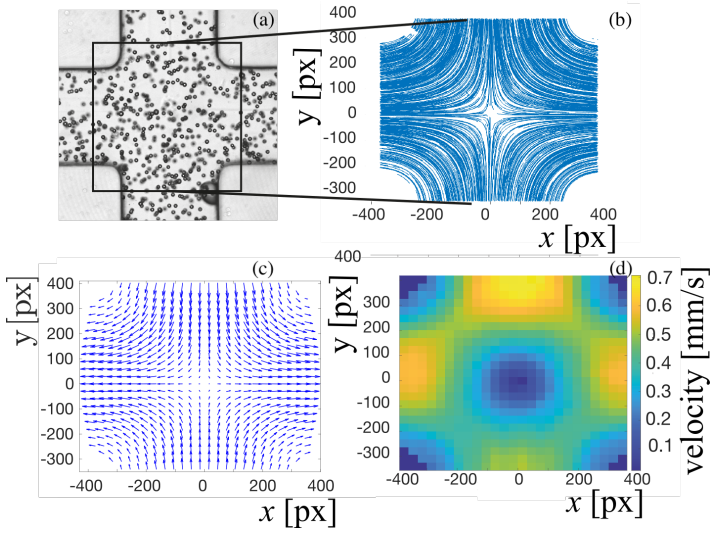

Fig. 3 (a) Picture of the flow in the presence of polystyrene particles. (b) Streamlines obtained by observing the particle flow during a long time. The data from (b) are treated using PIV to obtain the particles trajectories (c) and the velocity field (d).

Characterization of the velocity field in the extensional flow was carried out using polystyrene particles of diameter [50–80] μm mixed with the silicone oils of 500 and 1000 mPa s^{-1} (Fig. 3a). The flow is recorded for a specified time depending on the flowrate, high enough to observe the streamlines (15 s for $\dot{\varepsilon} = 1$ s^{-1}, Fig. 3b). The images are analyzed using Matlab PIV 2 codes to extract the particle trajectories (Fig. 3c) and the velocity field (Fig. 3d). Finally, we obtain a calibration of the shear rate as a function of the flowrate by fitting the variation of the velocity gradient by using a linear function (Fig. 4).

2.3 Drop deformation

The aim of the experiment is to link the drop deformation to the shear rate. We first define the gray level associated with the position of the droplet interface to automatically measure both the radius R of the drop in its spherical state and the lengths of the long and short axes (L and S) of the drop over time (Fig. 2c, inset). L and S values are extracted from the image at the moment when Taylor deformation is at its maximum. This ensures that the drop is trapped at the center of the elongational flow.

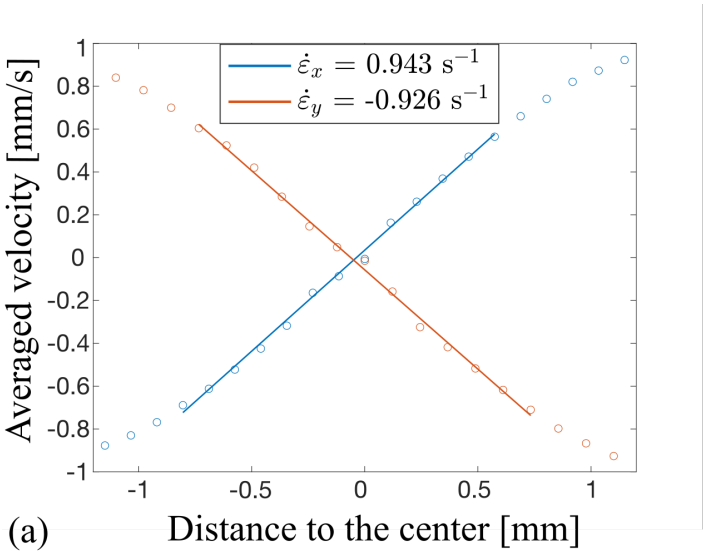

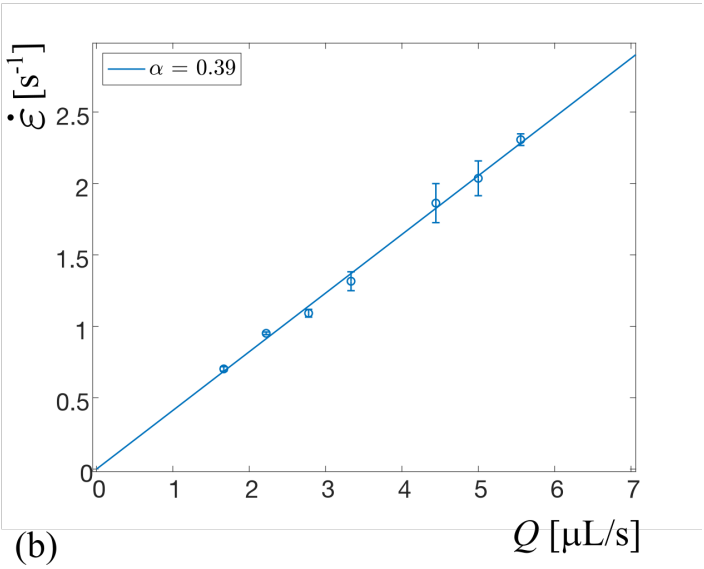

Fig. 4 (a) Velocity in the x and y directions, respectively, averaged and plotted as a function of the distance to the center of the flow. (b) Shear rate, obtained by fitting the velocity gradient as a function of the flowrate by a linear function.

3 Experimental results

3.1 Free interfaces

As stated in the Introduction, a droplet trapped at the center of an elongational flow is expected to undergo a deformation proportional to the capillary number Ca. In the case of an interface between two pure liquid phases, the prefactor Ξ (eqn (1)) is equal to 2. To validate our experimental setup in this simpler case, we plotted the deformation as a function of the capillary number (Fig. 5a). Since the surface tension is known with a low degree of precision, we adjusted the value of surface tension to obtain a slope equal to 2. This results in a surface tension $\gamma_0 = 21.2$ mN m^{-1}, which is in agreement within the uncertainties, with the sur-

face tension of 25.1 ± 6 mN m^{-1} measured by the pendant drop. This is equivalent to fixing the oil densities to 0.983 and 0.973 g cm^{-3} for the oils of viscosity to 1 Pa s and 0.5 Pa s respectively, which falls within the uncertainties of the densities given by the supplier data sheet. These densities will be used for all the experiments in the following, ensuring that relative variations of surface tension have a better accuracy than their absolute values. Note that in Fig. 5(a), the color bar denotes the bubble size. No systematic effect of this parameter is observed, demonstrating that no confinement effect is exhibited.

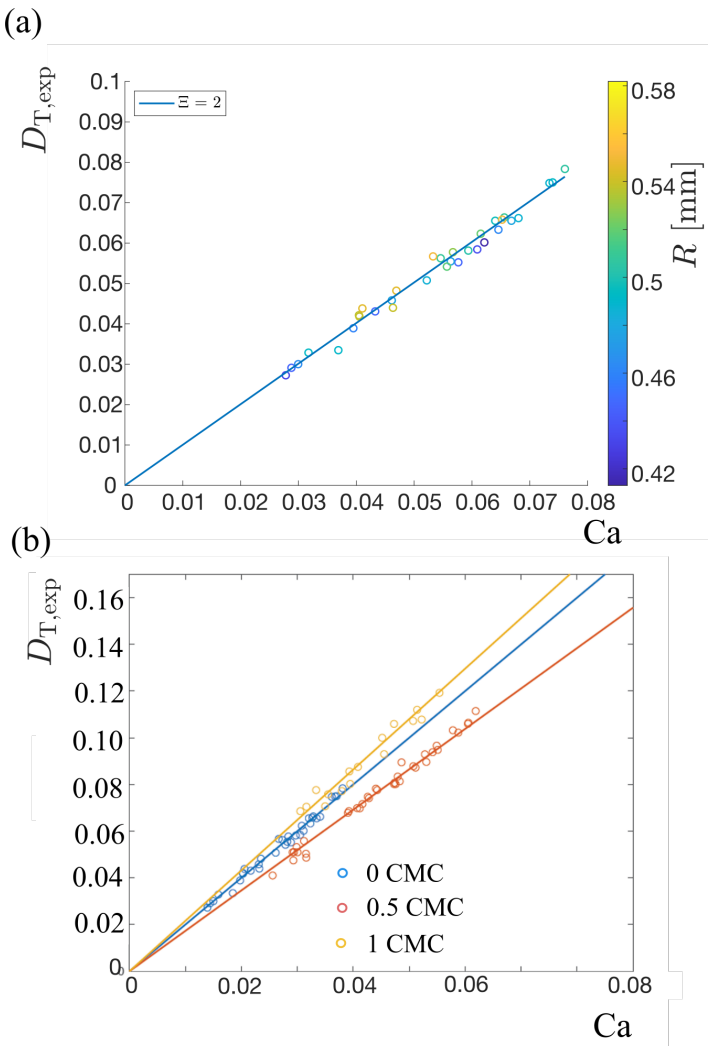

Fig. 5 (a) Taylor deformation as a function of the capillary number for different flowrates and different drop radii. The value of the oil density is adjusted to obtain the right surface tension for the slope of the continuous line to be 2 as predicted by Taylor.[7] (b) Taylor deformation measured for different flowrates and bubble sizes for C_{10}TAB at 0, 0.5 and 1 CMC. The continuous lines are obtained by fitting the data by a linear function. The slopes Ξ are plotted in Fig. 7.

3.2 Interfaces loaded by surfactants

In the following, the experiment has been performed on drops whose interfaces are loaded by surfactants. We varied both the surfactant system and the aqueous surfactant concentration. For each system, the Taylor deformation has been measured for different flow velocities and drop sizes, which allows us to vary the capillary number over more than an order of magnitude. The capillary number is built on the surface tension of the oil/surfactant solution interface, which is measured by the pendant drop using the density obtained in §2.1.3. A typical result is plotted in Fig. 5(b) for C_{10}TAB concentrations of 0, 0.5 and 1 CMC. The data always exhibit a linear behavior with Ca, as expected. They are fitted by a linear function to extract the prefactor Ξ, and depending on the experiment, we observe Ξ smaller or larger than 2. The difference between the data obtained at different concentrations is larger than the noise observed for each one, which makes us confident in the different slopes measured.

The data will be presented for each system by plotting Ξ as a function of the surfactant concentration. To evaluate the error bar on Ξ, we have measured $\Xi = D_T/\mathrm{Ca}$ for each drop and we have calculated the standard deviation of these results. In each figure, the value of the CMC is indicated by a vertical blue line.

For C_{14}TAB, the results are shown in Fig. 6 for the experiments with both the oil of viscosity 1 and 0.5 Pa s. For the continuous phase of higher viscosity, the prefactor decreases around the CMC to reach a minimum of around 1.2. At higher concentrations, it increases again to saturate at around 2 at concentrations above the CMC. This is in agreement with the results obtained by Lee *et al.*,[8] who used the method to measure surface tension at high surfactant concentrations, much above the CMC. Indeed, at high concentrations, the surfactant dynamics is expected to be negligible since the interfaces can be repopulated very rapidly when convection leads to a depleted zone. When the continuous phase has a smaller viscosity, the variation of Ξ is much smaller. Actually, in this case, the prefactor can always be considered to be equal to 2 within the error bars. This means that the effect of surfactant dynamics is almost suppressed by a low continuous phase viscosity.

We used a surfactant with a shorter hydrophobic chain, the C_{10}TAB to study the impact of surfactant dynamics. For C_{10}TAB, the results are plotted in Fig. 7 in the presence of the oil of viscosity 1 Pa s. The results are qualitatively very similar, with a prefactor Ξ close to 2 at small and high concentrations and reaching a minimum of 1.7 at a concentration close to but below the CMC. This surfactant is much more soluble in water than C_{14}TAB, which explains its much higher CMC (65 mM instead of 3.5 mM).

The behavior of the larger Gemini surfactant is qualitatively different. The results are plotted in Fig. 8, again using the oil of 1 Pa s viscosity. The variation of Ξ is much stronger than with the other surfactants. Ξ reaches a maximum close to 2.5 at low concentrations before decreasing to reach a minimum of 1.2 for a concentration close to but smaller than the CMC. The value of Ξ equal to 2.5 at small concentration is the signature of a regime, in which the surfactant can be described as an insoluble one.

Finally, our experimental results can be summarized as follows. In a pure liquid, we find experimental results compatible with the Taylor model. A finer comparison is delicate because of the larger uncertainties in the surface tension measurements using the pendant drop. We have measured the effect of the presence of sur-

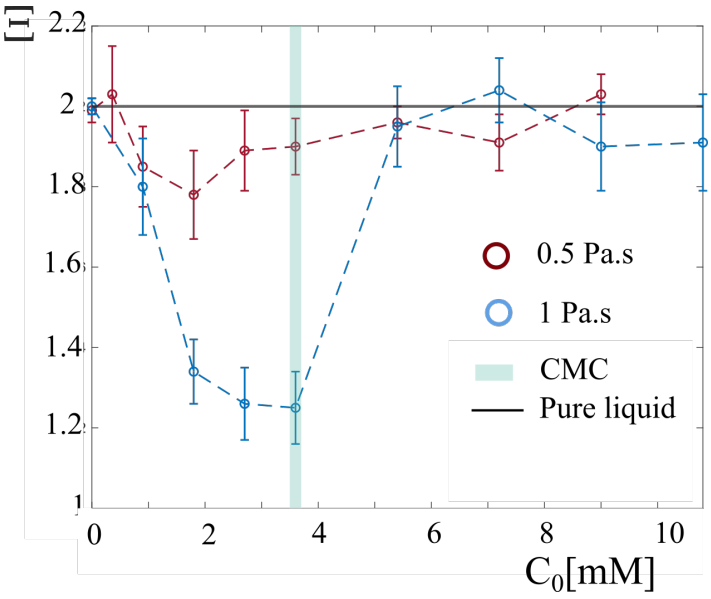

Fig. 6 Variation of Ξ with the surfactant concentration for C_{14}TAB. The vertical blue line represents the CMC, which is given in Table 1. The error bars are given by the standard deviation of Ξ, which can be measured for each experiment.

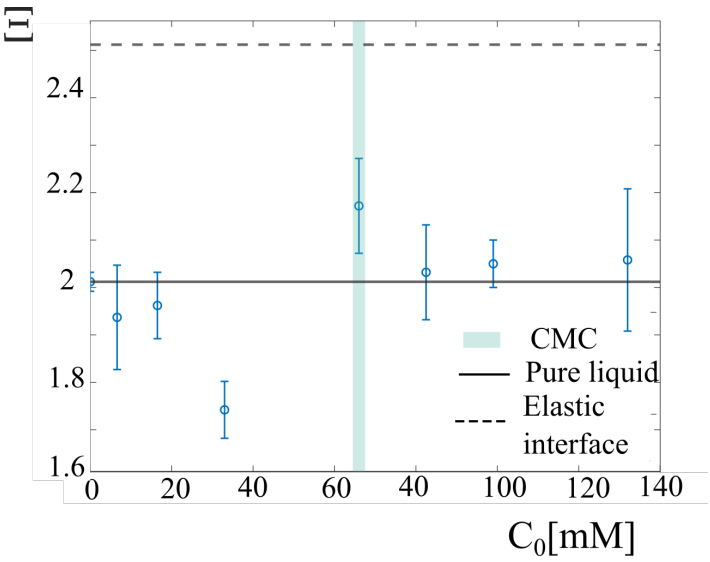

Fig. 7 Variation of Ξ with the surfactant concentration for C_{10}TAB. The vertical blue line represents the CMC, which is given in Table 1. The error bars are given by the standard deviation of Ξ, which can be measured for each experiment.

factants over a wide concentration range with systems with different solubilities. In all cases, at high concentrations, the slope tends to 2 and the pure liquid behavior is restored. This is consistent with an interpretation in which the interfaces are repopulated very rapidly at high concentrations, resulting in interfaces of homogeneous surface tension. There is a significant effect at intermediate concentrations for all surfactants in the presence of oil of viscosity $\eta = 1$ Pa s with a minimum value of Ξ smaller than 2. This result cannot simply be explained by the model proposed by Stone and Leal,[9] in which Ξ is always larger than 2. Unlike

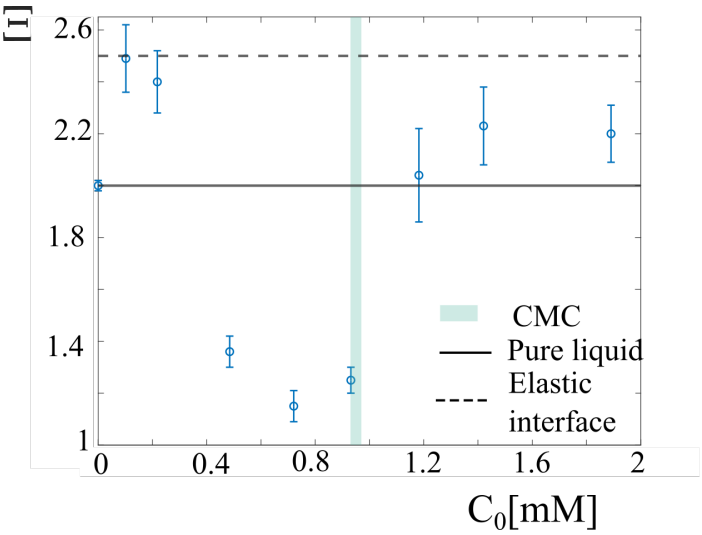

Fig. 8 Variation of Ξ with the surfactant concentration for the Gemini surfactant. The vertical blue line represents the CMC, which is given in Table 1. The error bars are given by the standard deviation of Ξ, which can be measured for each experiment.

the other two surfactants, for the Gemini surfactant, at very low concentrations, there is a regime in which the slope reaches the maximum value of 2.5 predicted by Leal and Stone.[9] Finally, for C_{14}TAB, we tested two different viscosities. We obtain an almost complete disappearance of the effect for a viscosity of 0.5 Pa s, half that used previously.

4 Model

4.1 Interface and perturbation

In the absence of flow, the droplet is a sphere of radius R as the energy is governed by surface tension. Under flow, the droplet deforms. To examine the effect of absorption-desorption of soluble surfactants on drop deformation, we adopt the same assumptions as those in the seminal works of Taylor, Stone, and Leal.[7,9] The system is analyzed within the framework of small deformations and under the low Reynolds number regime. The drop is assumed to be isolated (without wall interactions) and to have the same density as the surrounding fluid, thus neglecting buoyancy effects.

The position of its interface is determined in spherical coordinates as:

$$\boldsymbol{x}_I = r(\theta,\phi)\boldsymbol{e}_r, \tag{6}$$

where time has been omitted as we are only considering the final stationary state. Any surface function of (θ,ϕ) can be decomposed as an infinite sum of spherical harmonics, each representing a different type of deformation, see appendix in Boedec *et al.*[29] for details. Since the capillary number Ca is the main control parameter and as it is small, all the physical quantities are expanded linearly with Ca using the spherical harmonics $Y_{l,m}(\theta,\phi)$ as in previous studies.[9] For example, the radial position and the surface concentration of surfactants are

$$r = R\left(1 + \mathrm{Ca}\sum_{l,m} f_{l,m}Y_{l,m}\right) + O\left(\mathrm{Ca}^2\right), \tag{7}$$

$$\Gamma = \Gamma_{\mathrm{eq}} \left(1 + \mathrm{Ca} \sum_{l,m} g_{l,m} Y_{l,m} \right) + O\left(\mathrm{Ca}^2\right), \tag{8}$$

where l varies from zero to infinity while $-l \leq m \leq l$. $f_{l,m}$ and $g_{l,m}$ are the amplitudes of each mode (l,m) which only depend on the physical parameters. The experimental images correspond to the field of view $\theta = \pi/2$.

4.2 Surfactant dynamics

In the stationary state, the equation of conservation of the surfactant concentration C inside the droplet reads

$$(\boldsymbol{v}^{\mathrm{in}} \cdot \boldsymbol{\nabla}) C = D \Delta C, \tag{9}$$

where $\boldsymbol{v}^{\mathrm{in}}$ is the internal velocity and D is the coefficient of diffusion of free surfactants in the droplet. In the linear state, eqn (9) reduces to the Laplace equation, *i.e.*, $\Delta C = 0$.

In this study, we consider that surfactants can adsorb and desorb, obeying the kinetic model of Langmuir.[30–32] The derived results, however, are more general. Specifically, we investigate drop deformation in the regime of small deformations at leading order. Since the equations are linearized, any kinetic model will yield the same outcome. The chemical balance between adsorption and desorption at the interface is equal to the normal component of the volume flux $\boldsymbol{J}$ of surfactants :

$$\boldsymbol{J} \cdot \boldsymbol{n} = -K_1 C \left(1 - \frac{\Gamma}{\Gamma_\infty} \right) + K_2 \Gamma, \tag{10}$$

$$\boldsymbol{J} = -D \boldsymbol{\nabla} C + C \boldsymbol{v}^{\mathrm{in}}, \tag{11}$$

where $\boldsymbol{n}$ the unit normal vector, K_1 a kinetic constant characterizing the adsorption and K_2 the desorption. In the resting state, eqn (10) reduces to the Langmuir isotherm given by eqn (2) with

$$K_{\mathrm{L}} = \frac{K_1}{K_2 \Gamma_\infty}. \tag{12}$$

We introduce the ratio ψ_{eq} between the surface concentration in surfactants at equilibrium and the maximum one:

$$\psi_{\mathrm{eq}} = \frac{\Gamma_{\mathrm{eq}}}{\Gamma_\infty} = \frac{K_{\mathrm{L}} C_0}{1 + K_{\mathrm{L}}}. \tag{13}$$

In addition to kinetics, surfactants at the interface are also free to move along the interface by advection or diffusion satisfying this equation of conservation in the stationary state:

$$\begin{aligned} &\boldsymbol{\nabla}_s \cdot (\boldsymbol{v}_s \Gamma) + \Gamma (\boldsymbol{\nabla}_s \cdot \boldsymbol{n}) (\boldsymbol{v}_I \cdot \boldsymbol{n}) \\ &= D_s \Delta_s \Gamma + K_1 C \left(1 - \frac{\Gamma}{\Gamma_\infty} \right) - K_2 \Gamma, \end{aligned} \tag{14}$$

where D_s is the coefficient of surface diffusion, $\Delta_s (\equiv \boldsymbol{\nabla}_s \cdot \boldsymbol{\nabla}_s)$ the Laplace–Beltrami operator and $\boldsymbol{\nabla}_s = \left(I - \boldsymbol{n}\boldsymbol{n}^T\right) \cdot \boldsymbol{\nabla}$ is the surface gradient operator. $\boldsymbol{v}_s = (I - \boldsymbol{n}\boldsymbol{n}^T) \cdot \boldsymbol{v}_I$ is the in-plane surface velocity. The left member corresponds to the advective part, while the first term of the right member is the diffusive one. The difference with Stone and Leal[9] is the presence of the kinetic term.

4.3 Hydrodynamical equations

As previously mentioned, experiments are performed in the regime of low Reynolds number. The flow dynamics are thus described by the Stokes equations:

$$\begin{aligned} \Delta \boldsymbol{v}^{\mathrm{out}} &= \frac{1}{\eta^{\mathrm{out}}} \boldsymbol{\nabla} p^{\mathrm{out}}, \qquad \boldsymbol{\nabla} \cdot \boldsymbol{v}^{\mathrm{out}} = 0, \\ \Delta \boldsymbol{v}^{\mathrm{in}} &= \frac{1}{\eta^{\mathrm{in}}} \boldsymbol{\nabla} p^{\mathrm{in}}, \qquad \boldsymbol{\nabla} \cdot \boldsymbol{v}^{\mathrm{in}} = 0, \end{aligned} \tag{15}$$

with $\boldsymbol{v}$ the velocity of the fluid, p its pressure and η the viscosity. "in" and "out" indicate that the equation concerns respectively the pressure and velocity inside the drop or in the continuous phase. The boundary condition is

$$\lim_{r \to \infty} \boldsymbol{v}^{\mathrm{out}} = \boldsymbol{v}^{\infty}. \tag{16}$$

For a planar extensional flow, such boundary condition is

$$\boldsymbol{v}^{\infty} = \dot{\varepsilon} \left(x \boldsymbol{e}_x - y \boldsymbol{e}_y \right). \tag{17}$$

We assume that the velocities are continuous at the interface

$$\boldsymbol{v}_I = \boldsymbol{v}^{\mathrm{out}} = \boldsymbol{v}^{\mathrm{in}} \qquad \text{for } \boldsymbol{x} = \boldsymbol{x}_I. \tag{18}$$

In the stationary state, the surface velocities can only be tangential to the interface:

$$\boldsymbol{v}^{\mathrm{out}} \cdot \boldsymbol{n} = \boldsymbol{v}^{\mathrm{in}} \cdot \boldsymbol{n} = 0 \qquad \text{for } \boldsymbol{x} = \boldsymbol{x}_I, \tag{19}$$

Moreover, in addition to the velocity continuity, the fundamental equation of coupling between flow and interfacial properties is provided by the mechanical equilibrium at the interface:

$$\left(\boldsymbol{\Pi}^{\mathrm{out}} - \boldsymbol{\Pi}^{\mathrm{in}} \right) \cdot \boldsymbol{n} + \boldsymbol{F}_I = \boldsymbol{0} \qquad \text{for } \boldsymbol{x} = \boldsymbol{x}_I, \tag{20}$$

where $\boldsymbol{\Pi}$ is the hydrodynamic stress tensor and $\boldsymbol{F}_I$ the mechanical response of the interface to hydrodynamic jump by the contributions of Laplace contribution and surface tension gradients:

$$\boldsymbol{F}_I = -2\gamma H \boldsymbol{n} + \boldsymbol{\nabla}_s \gamma + \boldsymbol{f}_{\mathrm{visc,2D}}, \tag{21}$$

where $H = \boldsymbol{\nabla}_s \cdot \boldsymbol{n}/2$ is the mean curvature. Here, γ is the out-of-equilibrium surface tension which is assumed to be linked to the surface concentration Γ through the Szyszkowski equation (eqn (3)). The first term corresponds to a jump of pressure as in the Laplace equation, leading to a bulk flow if the curvature varies. The second one plays a role when the surface concentration of surfactants varies along the surface, leading to the so-called Marangoni effect. The third term $\boldsymbol{f}_{\mathrm{visc,2D}}$ takes into account the two-dimensional dissipation when considering the surface shear viscosity and the surface dilatational viscosity.

A classic way to write $\boldsymbol{f}_{\mathrm{visc,2D}}$ is to use the Boussinesq–Scriven tensor, as in recent analytical and numerical studies on droplets.[18,33,34] It is negligible in our case as the dissipation is dominated by the external viscosity. Indeed, the contribution of each surface viscosity can be evaluated by two dimensionless numbers B_q called Boussinesq numbers: $B_{qs} = \eta_s/\eta R$ and $B_{qd} = \eta_d/\eta R$ for shear (η_s) and dilatational (η_d) surface viscosi-

ties. In experiments, when the external viscosity is divided by 2, the Boussinesq numbers are multiplied by 2, whereas Ξ increases to be equal to 2 (Fig. 6), as for pure liquids. This is in contradiction with the expected impact of surface dissipation. In the following, this contribution is thus neglected.

4.4 Non-dimensional equations and solution

In the analytical derivation, the lengths, the time, the pressure, the bulk surfactant concentration C and its surface concentration Γ are made dimensionless considering the physical quantities R, $1/\dot{\varepsilon}$, $\eta\dot{\varepsilon}$, C_0 and $\Gamma_{\rm eq}$ respectively. In the following, dimensionless quantities are used.

One obtains

$$\left(\mathbf{\Pi}^{\rm out} - \lambda\, \mathbf{\Pi}^{\rm in}\right)\cdot\boldsymbol{n} = \frac{2}{\rm Ca}\left(1 - \frac{E_s\psi_{eq}}{\gamma_{\rm eq}}(\Gamma-1)\right)H\boldsymbol{n} + \frac{E_s\psi_{\rm eq}}{{\rm Ca}\gamma_{\rm eq}}\boldsymbol{\nabla}_s\Gamma. \tag{22}$$

In our experiments, the viscosity contrast $\lambda = \eta^{\rm in}/\eta^{\rm out} \approx 10^{-3}$ so that we choose to take $\lambda = 0$ in the following. The solution is determined at the first order in Ca. The zeroth order implies no deformation for the droplet and thus no flow at the interface. We multiply the evolution (eqn (14)) by $R^2/D_s\Gamma_{\rm eq}$ to obtain

$${\rm Ca}\zeta\boldsymbol{\nabla}_s\cdot\left(\Gamma\boldsymbol{v}_s^{\rm in}\right) + 2{\rm Ca}\zeta H(\boldsymbol{v}^{\rm in}\cdot\boldsymbol{n}) = \Delta_s\Gamma + \frac{K_1R^2C_0}{D_s\Gamma_{\rm eq}}C\left(1-\psi_{\rm eq}\Gamma\right) - \frac{K_2R^2}{D_s}\Gamma \tag{23}$$

with the non-dimensional quantities,

$$\zeta = \frac{\gamma R}{\eta^{\rm out}D_s},\ k_1^* = K_1\frac{R}{D_s},\quad k_2^* = K_2\frac{R^2}{D_s},\ \alpha = R\frac{C_0}{\Gamma_{\rm eq}}. \tag{24}$$

Such expressions are used to give a physical meaning to the kinetic quantities during resolution. ζ is the ratio of the surface diffusion time R^2/D_s over the viscous relaxation time $\eta^{\rm out}R/\gamma$ of an interface governed by a surface tension γ. It is also the ratio of the surface Peclet number over the capillary one. $k_1^* = (R^2/D_s)/(R/K_1)$ and $k_2^* = (R^2/D_s)/(1/K_2)$ compare the surface diffusion to adsorption and desorption kinetics respectively. α is a surface covering affinity comparing the number of surfactants present in the solution and the number of surfactants necessary to cover the interface. In the limit $\alpha << 1$, almost all the surfactants are at the interface and recalls the insoluble case while on the contrary, if $\alpha >> 1$, surfactants have a stronger affinity to the bulk.

Using eqn (18), (22), (19) and (14), the amplitudes $f_{l,m}$ and $g_{l,m}$ of eqn (7) and (8) are determined, leading to the Taylor parameter in the plane $\theta = \pi/2$: $D_{\rm T} = (L-S)/(L+S) = (r(\pi)-r(0))/(r(\pi)+r(0))$. It varies linearly with Ca

$$\frac{D_{\rm T}}{\rm Ca} = \Xi = \frac{5}{8}\frac{16 + 4\frac{E_s\psi_{\rm eq}}{\gamma_{\rm eq}}\zeta(1+\Lambda)}{5 + \frac{E_s\psi_{\rm eq}}{\gamma_{\rm eq}}\zeta(1+\Lambda)}. \tag{25}$$

The surface concentration is given by

$$\Gamma = 1 + {\rm Ca}\zeta\frac{5(1+\Lambda)}{10 + 2\frac{E_s\psi_{\rm eq}}{\gamma_{\rm eq}}\zeta(1+\Lambda)}\cos(2\phi), \tag{26}$$

with Λ a term coming from kinetic effects:

$$\Lambda = -\frac{1 + \frac{k_1^*}{k_2^*}\psi_{\rm eq}\alpha}{1 + \alpha\frac{k_1^*}{k_2^*}\psi_{\rm eq} - 3\frac{k_1^*}{k_2^*}\frac{D_s}{D}\left(1-\psi_{\rm eq}\right) + \frac{6}{k_2^*}}, \tag{27}$$

which can be recasted considering eqn (12)

$$\Lambda = -\frac{1 + K_{\rm L}C_0}{1 + K_{\rm L}C_0 - 3K_{\rm L}C_0\frac{D_s}{D}\frac{1-\psi_{\rm eq}}{\psi_{\rm eq}} + \frac{6}{k_2^*}} \tag{28}$$

A first examination of Λ shows that it can be positive or negative depending on the adsorption-desorption and diffusive parameters. If the internal diffusion of surfactants was omitted ($D \to 0$), there is no effect of kinetics as expected: $\Lambda \to 0$. In our experimental configuration, the ratio of diffusivities D/D_s is expected to be larger than 1 considering the Einstein relation for the diffusivity and the external viscosity higher than the internal one. The variation of the kinetic parameter Λ with $K_{\rm L}C_0$ is given in Fig. 9 considering that the typical time of desorption is slow compared to all other times, an expected limit. In this case, the kinetic parameter is negative leading to $1+\Lambda < 0$ in a large range of $K_{\rm L}C_0$. The transition ($\Lambda = -1$) corresponds to the limit of small surface coefficient of diffusion: $D_s << D$ and $k_2^\star = K_2R^2/D_s << 1$.

For $E_s = 0$ one recovers the usual Taylor deformation for planar extensional flow with a slope $\Xi = 2$ (Taylor[7]) if the variations of surface tension are high ($E_s\zeta >> \gamma_{\rm eq}$), the slope is equal to 2.5 (Vlahovska *et al.*[35]) as expected in the elastic limit. Without kinetics ($\Lambda = 0$), eqn (25) is the same as the one of Stone and Leal.[9] Finally $\Xi < 2$ is permitted by considering kinetic effects. As expected, adsorption-desorption kinetics only contribute when the equation of state (eqn (3) and (5)) depends on the surface concentration of surfactant. More accurately, in order to get the slope $\Xi = D_{\rm T}/{\rm Ca} < 2$ the quantity $\frac{E_s\psi_{\rm eq}}{\gamma_{\rm eq}}\zeta$ needs to be moderate (not a pure elastic response) and Λ must be smaller than -1. The variation of the slope with the dimensionless elastic number demonstrates a high sensitivity of the slope to small variations of the kinetic parameter as shown in Fig. 10 from $\Xi \approx 2.5$ to $\Xi \approx 1.3$. The addition of adsorption and desorption mechanisms modifies the classic point of view of interfaces only governed by surface elasticity which only allows $2 \le \Xi \le 2.5$ in partial disagreement with our observations.

5 Discussion

In the model, the deformation of a droplet is determined in the regime of low Reynolds number and in the limit of small capillary number taking into account the Langmuir model of adsorption-desorption kinetics and the Szyszkowski state equation. The slope $\Xi = D_{\rm T}/{\rm Ca}$, an essential feature in determining which physical effects dominate, varies in the range $1.3 \le \Xi \le 2.5$. As shown previously, the range $\Xi < 2$ is only allowed in the presence of kinetics. The droplet then becomes less deformable.

This is correlated with the sign of $1+\Lambda$ leading to an inver-

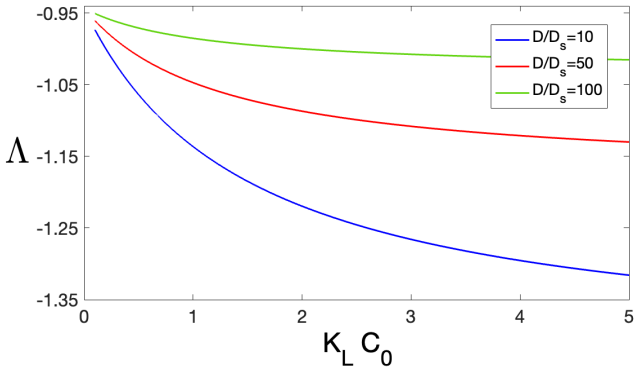

Fig. 9 Kinetic parameter Λ as a fonction of of $K_L C_0$ for different diffusive coefficients D/D_s. $\psi_{eq} = 0.5$, $k_2^* = 100$.

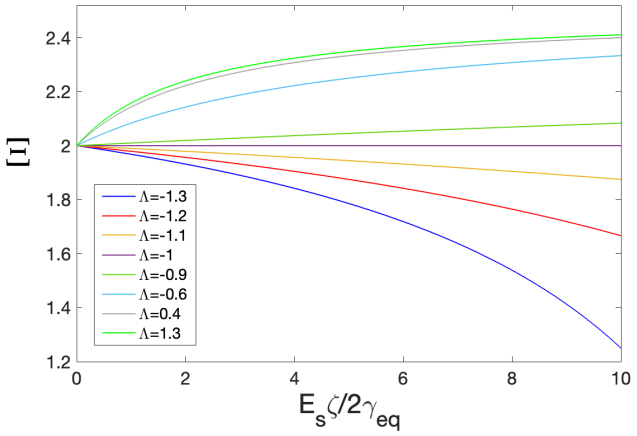

Fig. 10 Prefactor Ξ as a function of the elastic parameter $E_s\zeta/(2\gamma_{eq})$ for different values of Λ. $\psi_{eq} = 0.5$.

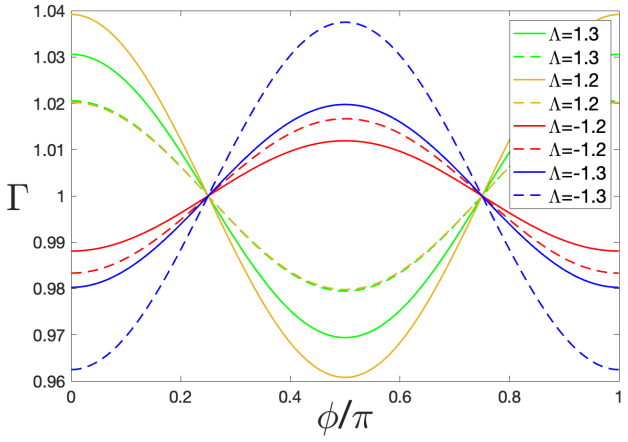

Fig. 11 Variation of the surface concentration of surfactants Γ along the surface. $\phi = 0, \pi$ correspond to the poles of the ellipsoid drop shape. $E_s\zeta/2\gamma_{eq} = 2$ (solid line), $E_s\zeta/2\gamma_{eq} = 5$ (dashed line). $\mathrm{Ca}\zeta = 0.1$

sion of the gradient of surfactant concentration compared to the regime governed by pure elasticity (eqn (26)). Indeed, in the regime described by Leal and Stone, the surfactants tend to accumulate at the pole, where they are entrained by convection: case $1+\Lambda > 0$ (Fig. 11). The smaller surface tension at the pole leads to an easier deformation. When $1+\Lambda$ becomes negative, eqn (26) shows that the surfactants actually accumulate at the equator (Fig.11) due to the bulk diffusion. This leads to the inverse effect, *i.e.*, a deformation smaller than for a pure liquid. The theoretical change of the Taylor parameter D compared to the well-known result of Stone and Leal[9] is only included in the kinetic parameter Λ. However, it is essential to see that the limit $D \to 0$ leads to $\Lambda = 0$. Without the internal diffusion of surfactants, *i.e.*, the redistribution of the surfactant concentration driving the internal diffusive flux, there is no such a non-intuitive effect of adsorption-desorption in the regime of low deformations. Finally, the following simple condition must be fulfilled to have a slope smaller than 2:

$$\frac{R^2}{D}(1-\psi_{eq}) > 2\frac{R}{K_1}, \tag{29}$$

Considering the initial eqn (27), it's interesting to be able to reduce such complexity to such a simple criterion. To our point of view, this reflects the simplicity of the model's basic equations and the limited number of characteristic times. As intuitively expected, a fast internal diffusivity compared to adsorption inhibits the process as internal concentration is homogenized. A consequence of our interpretation is the essential role of confinement, *i.e.*, that the surfactants are inside the drop. If the bulk surfactants are outside, they are entrained far from the droplet by the extensional flow, which prevents adsorption. Our analytical developments confirm this understanding. Indeed, the expression of the deformation with surfactants outside is the same as eqn (25) except that the quantity $1+\Lambda$ is now positive whatever the adsorption and desorption coefficients. For the sake of simplicity, these results will be presented elsewhere with an extension to general linear flows.[36] When the surfactant concentration is close to saturation ($\psi_{eq} \approx 1$), the condition revealed by eqn (29) is lost and the slope goes back to 2.

The theoretical predictions are difficult to compare directly with experiments. Indeed, in the literature, the measurements of the adsorption/desorption coefficients K_1 and K_2, the surface diffusion coefficient D_s and the equilibrium surface concentration Γ_{eq} are scarce and lack of accuracy. Nevertheless, the model allows to predict a slope Ξ smaller than 2 in the particular case, where $K_L \times C$ is larger than 0.5 as long as $\psi_{eq} \ll 1$. We have extracted the concentration $C^\star$ from the data in Fig. 6–8, at which the deformation is minimal. The error bars are given by the difference between the concentration just before and just after this transition.

This concentration $C^\star$ is plotted in Fig. 12 as a function of the value of $1/K_L$ listed in Table 1. Note that each point is for a different surfactant, condensing an extensive study, which accounts for the scarce sampling with three points in Fig. 12. The points extracted from our data suggest that the parameter $K_L C$ is indeed the right one to describe the small deformation observed at intermediate concentration. As the concentration increases and approaches the CMC, the interfaces is close to saturation, which releases one of the hypothesis necessary to observe a slope smaller than 2. This suggests that the physical reason, why we observe a

slope smaller than 2, is the fine balance between adsorption and desorption, predicted by the model. While the final analytical result may appear complex, the initial model is straightforward, with no intricate assumptions regarding the transport equation. For instance, the kinetic process is modeled in its simplest form. It is also worth noting that any more sophisticated model would yield the same result at leading order due to the linearization process.

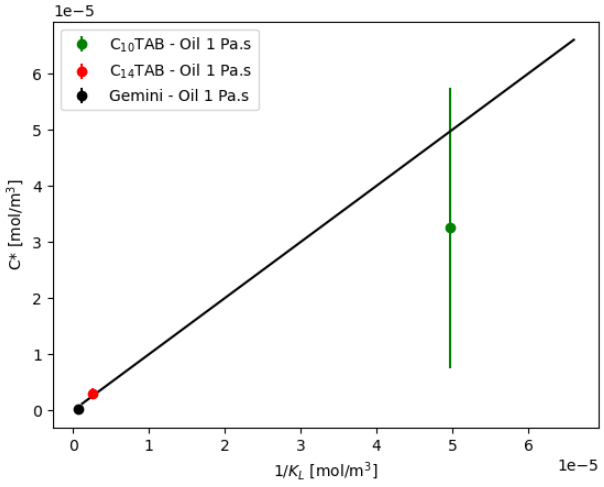

Fig. 12 Concentration measured at the minimal deformation, $C^\star$ as a function of the prediction $1/K_\mathrm{L}$.

6 Conclusion

We have performed an experiment allowing us to observe the deformation of a water drop immersed in oil in an extensional flow in the presence of surfactants. In the regime of small deformations and low Reynolds number, previous results suggested that the Taylor deformation varies linearly with the capillary number and that the slope can only range between 2 (pure liquids) and 2.5 (Gibbs elasticity of insoluble surfactants). We measured the Taylor deformation as a function of the velocity for different surfactant concentrations and systems. The recurrent observation is that the deformation is smaller than the one predicted for a pure liquid with the same surface tension, *i.e.*, a slope smaller than 2. Such a result cannot be explained by the seminal theoretical results of Taylor,[7] Stone and Leal[9] as it should do. Here, to propose a physical mechanism compatible with experiments, we consider the solubility of surfactants and the kinetic transfers at the surface (adsorption-desorption), which were not considered in previous models. We provide an analytical model, which predicts all the observed regimes, notably the one leading to a smaller deformation (slope smaller than 2). This new non-intuitive regime requires the surfactant solubility, low surfactant surface coverage and a bulk diffusion time larger than the characteristic adsorption time. Within these hypotheses, the deformation is driven by the surfactant bulk concentration through the parameter $K_\mathrm{L}C$, where K_L quantifies the adsorption/desorption dynamics. Our experimental data are in good agreement with this prediction, showing that the analytical model is able to describe qualitatively the observed experimental regime.

In this work, we have chosen to focus on surfactants with similar hydrophilic heads but significantly different solubilities. Experimentally, our results should be extended to different surfactant families, such as non-ionic or anionic types. Additionally, a complete comparison between experimental data and the model would require the measurement of certain parameters, which is still a challenge.

This would obviously be very useful to achieve a comprehensive and more quantitative description of dynamic interfaces. A key insight from this study is that surfactant solubilities and their dynamics can have a major impact even in simple configurations. We hope this work inspires further research to deepen understanding of interfacial dynamics involving soluble surfactants.

Data availability

Data for this article are available via the DOI: 10.5281/zenodo.13862518. Complementary data are available from the corresponding author upon reasonable request.

Conflicts of interest

There are no conflicts of interest to declare.

Acknowledgments

We acknowledge for funding support from the French Agence Nationale de la Recherche in the framework of project 2DVisc – ANR-18-CE06-0008-04 and from the CNES (through the GDR MFA). We thank Laura Wallon for measuring the liquid/liquid interfacial tensions, Sandrine Mariot for her help with the millifluidic device. We also would like to thank Cyprien Gay et Clément de Loubens for fruitful discussions and useful advice. We thank Martin In for giving us the dimeric surfactant.

Notes and references

1 D. Langevin, *Emulsions, microemulsions and foams*, Springer, 2020.
2 L. M. Sagis, *Rev. Mod. Phys.*, 2011, **83**, 1367–1403.
3 N. Jaensson and J. Vermant, *Curr. Opin. Colloid Interface Sci.*, 2018, **37**, 136–150.
4 D. Langevin, *Ann. Rev. Fluid Mech.*, 2014, **46**, 47–65.
5 S. Haward, *Biomicrofluidics*, 2016, **10**, 043401.
6 M. Q. Tu, H. V. Nguyen, E. Foley, M. I. Jacobs and C. M. Schroeder, *J. Rheol.*, 2023, **67**, 877–877.
7 G. I. Taylor, *Proc. R. Soc. London, Ser. A*, 1934, **146**, 501–523.
8 D. Lee and A. Q. Shen, *Micromachines*, 2021, **12**, 272.
9 H. A. Stone and L. G. Leal, *J. Fluid Mech.*, 1990, **220**, 161–186.
10 C. Tregouët, T. Salez, C. Monteux and M. Reyssat, *Soft Matter*, 2019, **15**, 2782–2790.
11 V. Kantsler, E. Segre and V. Steinberg, *Phys. Rev. Lett.*, 2008, **101**, 048101.
12 T. T. Perkins, D. E. Smith and S. Chu, *Science*, 1997, **276**, 2016–2021.

13 C. M. Schroeder, H. P. Babcock, E. S. Shaqfeh and S. Chu, *Science*, 2003, **301**, 1515–1519.
14 L. Guillou, J. B. Dahl, J.-M. G. Lin, A. I. Barakat, J. Husson, S. J. Muller and S. Kumar, *Biophys. J*, 2016, **111**, 2039–2050.
15 C. Trégouët, T. Salez, C. Monteux and M. Reyssat, *Phys.Rev. Fluids*, 2018, **3**, 053603.
16 Q. Brosseau, J. Vrignon and J.-C. Baret, *Soft Matter*, 2014, **10**, 3066–3076.
17 C. De Loubens, J. Deschamps, G. Boedec and M. Leonetti, *J. Fluid Mech.*, 2015, **767**, R3.
18 R. W. Flumerfelt, *J. Colloid and Interface Sci.*, 1980, **76**, 330–349.
19 J. Eastoe and J. Dalton, *Adv. Colloid Interface Sci.*, 2000, **85**, 103–144.
20 C. D. Eggleton and K. J. Stebe, *J. Colloid and Interface Sci.*, 1998, **208**, 68–80.
21 C. D. Eggleton, Y. P. Pawar and K. J. Stebe, *J. Fluid Mech.*, 1999, **385**, 79–99.
22 Y. Pawar and K. J. Stebe, *Phys. Fluids*, 1996, **8**, 1738–1751.
23 W. Milliken and L. Leal, *J. Non-Newtonian Fluid Mech.*, 1991, **40**, 355–379.
24 W. Milliken, H. A. Stone and L. Leal, *Phys. Fluids A*, 1993, **5**, 69–79.
25 Y. Hu and A. Lips, *Phys. Rev. Lett.*, 2003, **91**, 044501.
26 C. Stubenrauch and K. Khristov, *J. Colloid and Interface Sci.*, 2005, **286**, 710–718.
27 M. In, V. Bec, O. Aguerre-Chariol and R. Zana, *Langmuir*, 2000, **16**, 141–148.
28 A. Daerr and A. Mogne, *J. Open Res. Software*, 2016, **4**, e3.
29 G. Boedec, M. Jaeger and M. Leonetti, *J. Fluid Mech.*, 2012, **690**, 227–261.
30 P. A. Kralchesky and K. Nagayama, *Particles at fluid interfaces and membranes*, Elsevier, 2001.
31 J. Baret, *J. Colloid and Interface Sci.*, 1969, **30**, 1–12.
32 H. Manikantan and T. M. Squires, *J. Fluid Mech.*, 2020, **892**, P1.
33 J. Gounley, G. Boedec, M. Jaeger and M. Leonetti, *J. Fluid Mech.*, 2016, **791**, 464–494.
34 V. Narsimhan, *J. Fluid Mech.*, 2019, **862**, 385–420.
35 P. M. Vlahovska, J. Bławzdziewicz and M. Loewenberg, *J. Fluid Mech.*, 2009, **624**, 293–337.
36 P. Regazzi and M. Leonetti, *submitted*, 2024.